RESEARCH ARTICLE | MAY 25 2023

Wind-driven transport on the rotating spherical Earth

N. Paldor ✉ ; L. Friedland

Physics of Fluids 35, 056604 (2023)
https://doi.org/10.1063/5.0151488

Physics of Fluids ARTICLE pubs.aip.org/aip/pof

Wind-driven transport on the rotating spherical Earth

Cite as: Phys. Fluids **35**, 056604 (2023); doi: 10.1063/5.0151488
Submitted: 22 March 2023 · Accepted: 9 May 2023 ·
Published Online: 25 May 2023

View Online Export Citation CrossMark

N. Paldor[1,a)] and L. Friedland[2]

AFFILIATIONS

[1]Fredy and Nadine Herrmann Institute of Earth Sciences, Hebrew University of Jerusalem, Jerusalem, Israel
[2]Racah Institute of Physics, Hebrew University of Jerusalem, Jerusalem, Israel

[a)]Author to whom correspondence should be addressed: nathan.paldor@mail.huji.ac.il

ABSTRACT

The dynamics of a water column at the surface of the ocean on the rotating spherical Earth forced by zonal wind stress is analyzed by substituting the angular momentum for the zonal velocity as one of the system's dependent variables. This substitution results in a model of the column's trajectory as a quasiparticle in a time dependent potential well. Explicit solutions are derived for the temporal changes in the angular momentum and the associated minima of the potential well as well as for the oscillations about these minima. The analytic results are confirmed by numerical solutions of the fourth-order nonlinear system of ordinary differential equations. For the eastward directed wind stress, our results provide exact formulas for the time it takes a column to reach the equator, where the dynamics is trivially described by the non-rotating paradigm of a particle subject to a constant force. In mid-latitudes, the analysis underscores the pivotal role played by the latitude where the wind-stress changes sign. Columns originating north or south of this latitude either converge to it or diverge away from it depending on whether the latitudinal change of the wind stress at this latitude is positive or negative. The oscillatory motion about this latitude is linearly unstable, and the growth rate of the amplitude is proportional to the gradient of the wind stress at that latitude.

I. INTRODUCTION

The fundamental theory describing the circulation in the ocean upper layer forced by the wind blowing over the ocean was developed by Ekman in 1905[1] in Cartesian coordinates and for constant Coriolis frequency, a setup termed today—the *f*-plane. This concise and elegant linear theory employs the Lagrangian form of the vertically averaged fluid dynamical equations to calculate the trajectory of a water column of height h at the ocean surface. Ekman showed that the trajectory of the column consists of a steady flow at right (left, in the southern hemisphere) angle to the wind direction compounded by linear oscillations at the (constant) Coriolis frequency.

The addition of the latitudinal gradient of the Coriolis frequency, known as the β-effect, introduces nonlinear terms in the equations and introduces a latitude where the Coriolis frequency vanishes—the equator. The changes in the water column trajectory caused by the β-effect were examined in Ref. 2 who showed that a (slow) drift parallel to the wind direction is added to the *f*-plane trajectory when the β term is added to the governing equations. This drift of water columns parallel to the wind direction was never shown to prevail in spherical coordinates.

Though rarely employed, the Lagrangian form of fluid dynamics was successfully used in geophysical fluid dynamics (GFD) to elucidate subtle aspects in some particular problems, such as the westward drift of inertial flows on the β-plane[3,4] and on the sphere.[5,6] In this context, the extension of Ekman's *f*-plane theory to spherical coordinates follows the procedure employed in previous extensions of the inertial dynamics to spherical coordinates.

Prior studies of the wind-driven ocean dynamics in spherical coordinates were primarily numerical[7] or employed nonlinear Eulerian formulation to establish a unified view of the equatorial and mid-latitude dynamics.[8] In contrast, in the present study, we present a dynamical system view of the wind-driven circulation in spherical coordinates. As in all previous studies on the subject of wind-driven transport in the upper ocean, the analysis in the present spherical setup is restricted to zonal wind-stress forcing (of different forms) as in the climatological winds on Earth. The analysis of the less frequent, meridional, stresses is left to future works. The title of this paper deserves an explanation. Though spherical coordinates are used, the centrifugal acceleration in the momentum equations is ignored. This is justified because Earth's surface is closer to an oblate spheroid than to

a prefect sphere (which is the origin of the "equatorial bulge"). The slight deviation from a perfect sphere induces a poleward directed tangential component of the gravitational acceleration that balances the outward (relative to Earth's axis of rotation) directed centrifugal acceleration. The term "rotating spherical Earth" is used here to denote a rotating sphere, in which the centrifugal acceleration is neglected along with the slight eccentricity of the oblate spheroid.

Our theory focuses on the case of weak zonal stress, which introduces a small parameter in the problem that allows the use of a perturbative analysis. Using the Wentzel–Kramers–Brillouin (WKB) method for oscillatory systems with slow parameters (see, for example, Ref. 9), we show that in spherical coordinates, a water column forced by zonal stress undergoes a slow monotonic time evolution with superimposed small amplitude, large frequency, modulations. The resulting water column trajectories vary qualitatively from those forced with the same wind forcing on the β-plane.

This paper is organized as follows. We develop the model nondimensional equations including the use of the angular momentum as a state variable in Sec. II. In Sec. III, we formulate the equations describing the temporal evolution of the potential of the meridional dynamics, including the evolution of the angular momentum. The dynamics is separated into the temporal changes in the slow (mean) variables and the fast oscillations about them. This is followed in Sec. IV by a WKB analysis and solution of the combined angular-momentum and meridional dynamics system. The longitudinal dynamics is formulated, and solution for the averaged motion is developed in Sec. V. In Sec. VI, we solve the problem for additional meridional structures of the overlying wind-stress forcing, including the case of a wind stress that changes sign at a certain latitude. The paper is concluded with a summary and discussion in Sec. VII.

II. MODEL EQUATIONS

The horizontal, vertically averaged, Lagrangian dynamics of a water column at the ocean surface forced by the overlying zonal wind stress is determined by the rotating shallow water equations (RSWE), in which a suitable forcing term is added to the zonal momentum equation.[7,10,11] Denoting the latitude-dependent zonal wind stress by τ^x and the surface layer thickness by h, the zonal wind forcing is given by $\frac{\tau^x}{\rho h}$, where ρ is the water density. The natural scales of the RSWE in spherical coordinates are time on 2Ω (where Ω is the frequency of Earth's rotation), velocity on $2R_e\Omega$ (where R_e is Earth's mean radius—the obvious length scale), and acceleration on $(2\Omega)^2R_e$. These scales yield the following nondimensional system:

$$\frac{du}{dt} = v\sin\varphi\left(1+\frac{u}{\cos\varphi}\right)+\Gamma, \tag{1}$$

$$\frac{dv}{dt} = -u\sin\varphi\left(1+\frac{u}{\cos\varphi}\right), \tag{2}$$

$$\frac{d\lambda}{dt} = \frac{u}{\cos\varphi}, \tag{3}$$

$$\frac{d\varphi}{dt} = v, \tag{4}$$

where u and v are the vertically averaged velocity components in the zonal (angle—λ) and meridional (angle—φ) directions, respectively, and $\Gamma(\varphi) = \frac{\tau^x(\varphi)}{h\rho(2\Omega)^2R_e}$ is the nondimensional zonal wind forcing. For realistic values of τ^x (0.1 Pa) and h (50 m), $\Gamma \approx 1.5\times10^{-5}$, so the theory developed here assumes $\Gamma \ll 1$.

Equations (1) and (4) imply that the rate of change of the nondimensional total angular momentum (defined as $D = \frac{1}{2}\cos^2\varphi + u\cos\varphi$) is given by

$$\frac{dD}{dt} = \Gamma\cos\varphi. \tag{5}$$

Since the wind stress appears only in this equation where it determines the rate of temporal change in D, in the numerical examples here we use larger values of wind stress [i.e., $O(10^{-3})$] to expedite the time of integration. The inverse of the $D(u)$ relation, $u = \frac{D}{\cos\varphi} - \frac{1}{2}\cos\varphi$, can be employed to eliminate u from the system so it transforms to

$$\frac{dv}{dt} = \frac{1}{2}\sin(2\varphi)\left(\frac{1}{4}-\frac{D^2}{\cos^4\varphi}\right), \tag{6}$$

$$\frac{d\lambda}{dt} = \frac{D}{\cos^2\varphi}-\frac{1}{2}, \tag{7}$$

$$\frac{d\varphi}{dt} = v. \tag{8}$$

The substitution of D for u enables a novel physical interpretation of the φ-dynamics, which greatly simplifies the analysis in the rest of this work.

III. THE EVOLUTION OF φ

We proceed with the examination of the φ (i.e., meridional) part of the dynamics described by Eqs. (5), (6), and (8), rewritten as

$$\frac{d^2\varphi}{dt^2} = \frac{1}{2}\sin(2\varphi)\left(\frac{1}{4}-\frac{D^2}{\cos^4\varphi}\right), \tag{9}$$

$$\frac{dD}{dt} = \Gamma(\varphi)\cos\varphi, \tag{10}$$

where the zonal wind stress is a function of φ. The initial conditions to be employed are $\varphi(0) = \varphi_0$ (with an arbitrary $-\pi/2 \le \varphi_0 \le \pi/2$), $v(0) = v_0$ is small, and $D(0) = D_0 = \frac{1}{2}\cos^2\varphi_0 + u(0)\cos\varphi_0$, where $u(0)$ is small.

The analysis in the rest of the paper focuses on the case of sufficiently small zonal wind forcing $\Gamma = GF(\varphi)$, where $G \ll 1$ and $F(\varphi)$ is $O(1)$. The smallness of G suggests a perturbative analysis. For zeroth order, i.e., for $G = 0$, Eq. (10) implies that the angular momentum, D, remains *constant* in time and the dynamics of φ is described by

$$\frac{d^2\varphi}{dt^2} = -\frac{\partial\Phi}{\partial\varphi}, \tag{11}$$

where

$$\Phi = \frac{1}{2}\left[\frac{D}{\cos\varphi}-\frac{1}{2}\cos\varphi\right]^2. \tag{12}$$

In other words, the evolution of φ can be interpreted as the motion of a quasiparticle in the potential well Φ. This motion is determined by the form of the potential well and the initial conditions. The extrema of this potential are given by the roots of

$$\left(\frac{D}{\cos\varphi}-\frac{1}{2}\cos\varphi\right)\left(\frac{D}{\cos^2\varphi}+\frac{1}{2}\right)\sin\varphi = 0. \tag{13}$$

Thus, for $0 < D < 1/2$, two minima exist, which are located at $\cos\varphi_m = \pm\sqrt{2D}$ (the solution with $\cos\varphi_m = -\sqrt{2D}$ is not acceptable in our model where $-\pi/2 \le \varphi \le \pi/2$), and the local maximum is located at $\varphi_m = 0$. In contrast, for $D > 1/2$, the single extremum is a global minimum located at $\varphi = 0$. We illustrate this potential in Fig. 1 for ten values of $D = 0.1i$ (where $i = 1, 2, \ldots, 10$). The figure clearly demonstrates the transition from two minima for $D < 1/2$ (blue lines) to a single minimum for $D > 1/2$ (red lines).

Turning to the initial conditions, we note that $\varphi(0) = \varphi_0$ and small $u(0)$ imply that $D = \frac{1}{2}\cos^2\varphi_0 + u(0)\cos\varphi_0 \approx \frac{1}{2}\cos^2\varphi_0$. Therefore, φ_0 is located near the local minimum of Φ, as described above. Consequently, to lowest order in the small parameter G, the solution for φ is made up of *small* oscillations $\delta\varphi$ around the minimum of the potential, φ_m, i.e., $\varphi = \varphi_m + \delta\varphi$. This inertial dynamics was studied in depth in spherical coordinates by Refs. 12–14, and the highly chaotic nature of slight deviations from this idealized case is highlighted in Refs. 6 and 15.

To first order in $G \ll 1$, we seek solutions of the (φ, D) system in the form $D = D_m(t) + \delta D$ and $\varphi = \varphi_m(t) + \delta\varphi$ where δD and $\delta\varphi$ are small. The definition of $\varphi_m(t)$ is the location of the minimum of the potential Φ, in which D is replaced by $D_m(t)$, i.e., $\cos^2\varphi_m(t) = 2D_m(t)$, while $D_m(t)$ evolves according to

$$\frac{dD_m}{dt} = GF(\varphi_m)\cos\varphi_m. \tag{14}$$

With these definitions, this equation implies that $D_m(t)$, and hence $\varphi_m(t)$, varies *slowly* with time (on $1/G \gg 1$ timescale). Furthermore, by expanding Eqs. (9) and (10) to first order in δD and $\delta\varphi$ and neglecting the $O(G^2)$ term $d^2\varphi_m/dt^2$ in Eq. (9), we get

$$\frac{d^2\delta\varphi}{dt^2} = -\omega_m^2\delta\varphi - Q\delta D, \tag{15}$$

$$\frac{d\delta D}{dt} = GP(\varphi_m)\delta\varphi, \tag{16}$$

where $Q = 2D_m \sin\varphi_m/\cos^3\varphi_m$, $P = \partial[F(\varphi_m)\cos\varphi_m]/\partial\varphi_m$, and for $\varphi_m > 0$ (i.e., $D_m < 1/2$),

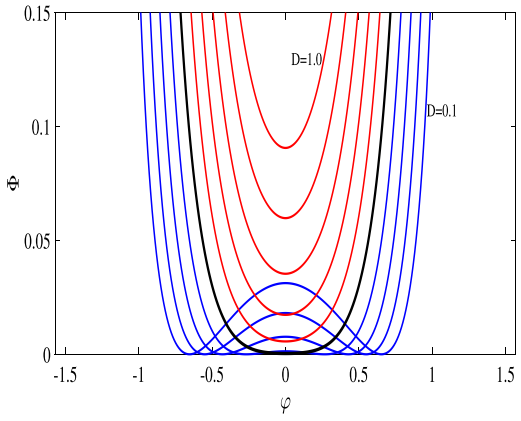

FIG. 1. Snapshots of the potential well $\Phi(\varphi, D)$ for ten values of $D = 0.1i (i = 1, 2, \ldots, 10)$. The potential has two minima for $D < 0.5$ (blue lines) and a single minimum at $\varphi = 0$ for $D > 0.5$ (red lines). The black line corresponds to the critical transition value of $D_{cr} = 0.5$.

$$\omega_m^2 = 1 - 2D_m = \sin^2\varphi_m. \tag{17}$$

[Note: The case $\varphi_m = 0$, where the potential has a single minimum (see Fig. 1), is discussed below.] Equations (14)–(16) comprise a complete set describing the evolution of φ and D to first order in our perturbation scheme. The qualitative change in the potential when φ_m reaches the equator, which is clearly demonstrated in Fig. 1, mandates that the off-equatorial dynamics (i.e., short times) be analyzed separately from the equatorial (longtime) dynamics. We conclude this section by discussing the slow time evolution of D_m for the simple case of constant $\Gamma = G$ and postpone the analyses of the evolution of δD and $\delta\varphi$ in Sec. IV.

In the simple, $\Gamma = G$, case and when $\varphi_m > 0$, the temporal changes in D can be found by solving Eq. (14), i.e., $dD_m/dt = G\sqrt{2D_m}$, which yields solution

$$D_m(t) = \left(\sqrt{D_m(0)} + \frac{Gt}{\sqrt{2}}\right)^2. \tag{18}$$

Thus, for $G > 0$, the value of D_m increases initially from its initial value of $D_m(0) \approx \frac{1}{2}\cos^2\varphi_0 < \frac{1}{2}$ until it reaches the critical value of $D_{cr} = \frac{1}{2}$ near the equator (i.e., $\varphi = 0$). Substituting $\frac{1}{2}$ on the LHS of Eq. (18) yields an expression for the (critical) time for the minimum φ_m (and the column) to reach the equator

$$t_{cr} = \frac{1 - \sqrt{2D_m(0)}}{G} = \frac{1 - \cos\varphi_m(0)}{G}. \tag{19}$$

For $t < t_{cr}$, φ evolves around the minimum $\varphi_m(t) > 0$ of the potential. In contrast, for $t > t_{cr}$, $D_m(t) > 1/2$ and $\varphi(t)$ oscillates about the equator ($\varphi_m = 0$) so

$$\omega_m^2 = D_m^2 - \frac{1}{4}, \tag{20}$$

$$D_m = \frac{1}{2} + G(t - t_{cr}). \tag{21}$$

We illustrate this evolution in Fig. 2. The left panel in Fig. 2 shows the temporal evolution of $\varphi(t)$ obtained numerically for $\Gamma = 0.005$ and initial conditions $\varphi(0) = \pi/4$, $u(0) = 0$, $v(0) = 0.02$ and $\lambda(0) = 0$, and the right panel presents the geographical, (λ, φ), trajectory until λ reaches the value of 0.1 (at time $t = 60.13$, a tad above $t_{cr} = 58.6$). These results show that as predicted above, the character of evolution changes qualitatively when time passes the critical time $t_{cr} = 58.6$. Figure 2 also demonstrates that the trajectory oscillates around φ_m, while the location of this minimum moves (toward the equator when $\Gamma > 0$) in response to the time variation of D.

Many of the flow characteristics under non-uniform $\Gamma(\varphi)$ profiles are also encountered in the highly idealized case of constant Γ. The evolution of $D_m(t)$ in these cases is determined similarly by solving Eq. (14), where $\cos\varphi_m = \sqrt{2D_m}$ for $t < t_{cr}$ and $\varphi_m = 0$ for $t > t_{cr}$. Examples of nonuniform $\Gamma(\varphi)$ are discussed in detail in Sec. VI.

IV. WKB ANALYSIS OF THE $(\delta D, \delta\varphi)$ SYSTEM

The dynamics of oscillations of $\delta\varphi$ and δD around the slowly varying mean variables φ_m and D_m is described by the linear system (15) and (16) with known and slowly varying coefficients (Q, P, ω_m^2), as described in Sec. III. To solve these equations, we employ the WKB method, seeking the eikonal ansatz

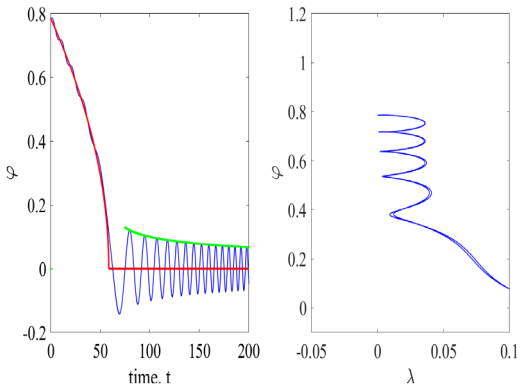

FIG. 2. Results of constant Γ case with $\Gamma = 0.005$, $\varphi(0) = \pi/4$, $u(0) = 0$, $v(0) = 0.02$, and $\lambda(0) = 0$. Left panel: the temporal evolution of $\varphi(t)$ (blue curves), and the red line shows the evolution of ϕ_m. The green line shows the predicted time variation of the amplitude of oscillations of φ from the action conservation formula [see Eq. (29) with I = 0.01]; right panel: the geographical, (λ, φ) trajectory (blue curves). The trajectories on the right panel terminate when λ reaches the value of 0.1 at time $t = 60.13$, right above $t_{cr} = 58.6$, the critical time for these parameters according to Eq. (19). Each panel includes two blue curves, one derived from exact numerical simulations and the other using the approximate formula, in which D is replaced by D_m. The numerical and analytic curves can barely be distinguished from one another.

$$\delta\varphi = Re\left(ae^{i\int \omega dt}\right), \quad \delta D = Re\left(be^{i\int \omega dt}\right), \tag{22}$$

where ω is $O(1)$, and the small amplitudes a and b and ω vary slowly with time. For this form of solution, Eqs. (15) and (16) yield

$$i\frac{d(a^2\omega)}{dt} = (\omega^2 - \omega_m^2)a^2 - Qab, \tag{23}$$

$$i\omega b + \frac{db}{dt} = GPa, \tag{24}$$

where we have neglected the $O(G^2)$ term ad^2a/dt^2 in Eq. (23). Next, we neglect the relatively small term db/dt in Eq. (24) and combine the result with Eq. (23) into a single equation,

$$i\frac{d(a^2\omega)}{dt} = \left(\omega^2 - \omega_m^2 - i\frac{GQP}{\omega}\right)a^2. \tag{25}$$

Since in our WKB representation, Eq. (22), the single function $\delta\varphi$ is defined by two functions a and ω, we are free to choose one of these functions at our will. We use this freedom to define ω by

$$\omega^2 - \omega_m^2 - i\frac{GQP}{\omega} = 0, \tag{26}$$

which yields the solution

$$\omega \approx \omega_m + \nu, \tag{27}$$

where the small imaginary part of the frequency is

$$\nu = -i\frac{GQP}{2\omega_m^2}. \tag{28}$$

In addition, for the solution described by Eq. (26), Eq. (25) yields the usual adiabatic invariant of a linear oscillator with slowly varying frequency,

$$I = a^2\omega_m \approx const. \tag{29}$$

Thus, the full solutions for $\delta\varphi$ and δD are

$$\delta\varphi = A\cos\int \omega_m dt, \quad \delta D = \frac{GP}{\omega_m}A\sin\int \omega_m dt, \tag{30}$$

where A is the slowly varying amplitude given by

$$A = \sqrt{\frac{I}{\omega_m}}e^{G\int\frac{QP}{2\omega_m^2}dt}. \tag{31}$$

As an example, we apply this theory to the simplest case of uniform $\Gamma = G$. In this case, for $t < t_{cr}$,

$$Q = \frac{2D_m\sin\varphi_m}{\cos^3\varphi_m} = \tan\varphi_m, \quad P = -\sin\varphi_m = -\sqrt{1 - 2D_m},$$

and for $t > t_{cr}$, $Q = P = 0$. Thus, the power of the exponent in Eq. (31) is either negative or vanishes. In the examples of Figs. 2 and 3, we can see the slow evolution of φ_m (red lines), the oscillation $\delta\varphi$ as predicted in Eq. (30), as well as the adiabatic variation of the oscillations' amplitude (the green lines) that decreases in accordance with the increase in frequency anticipated by Eqs. (20) and (21). Note that the adiabaticity assumption of the theory breaks down when the frequency of oscillation approaches zero, i.e., near $t = t_{cr}$. Indeed, we observe the nonadiabatic jump in the amplitude at this critical time. We will analyze other cases of nonuniform Γ in Sec. VI, but first we discuss, in Sec. V, the zonal drift.

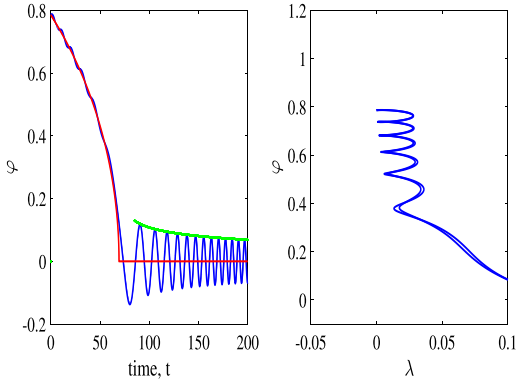

FIG. 3. Summary of numerical results for $\Gamma = G\cos\varphi$ with $G = 0.005$ and the same initial conditions as in Fig. 2. Left panel: the temporal evolution of $\varphi(t)$; the red line shows the evolution of ϕ_m. The green line shows the predicted time variation of the amplitude of oscillations of φ from the action conservation formula [see Eq. (29) with I = I = 0.0049]. Right panel: geographical $(\lambda, \varphi$, trajectory for $\lambda \leq 0.1$, i.e., during the time when the trajectory is away from the equator). For the values of Γ and φ_0 used here, Eq. (38) yields a critical time of $t_{cr} = 69.3$. Each of the panels contains two blue curves, one obtained from numerical integration of system 1–4 and the other from the approximate analytic solutions, in which D is replaced by D_m.

V. THE EVOLUTION OF λ (ZONAL DRIFT)

The zonal part of the dynamics is determined by Eq. (7),

$$\frac{d\lambda}{dt} = \frac{D}{\cos^2\varphi} - \frac{1}{2}. \tag{32}$$

As in the meridional analysis of Sec. IV, we let $\varphi = \varphi_m + \delta\varphi$ and $D = D_m + \delta D$ and expand the RHS in powers of $\delta\varphi$ and δD keeping only terms of second order or lower in the amplitudes a and b. For the case $t < t_{cr}$, the result is

$$\frac{d\lambda}{dt} = \gamma_1\delta\varphi + \gamma_2\delta D + \gamma_3\delta\varphi^2 + \gamma_4\delta\varphi\delta D, \tag{33}$$

where

$$\gamma_1 = \left(\frac{1}{2D_m} - 1\right)^{1/2}, \quad \gamma_2 = \frac{1}{2D_m},$$
$$\gamma_3 = -1 + \frac{3}{4D_m}, \quad \gamma_4 = \frac{1}{D_m}\sqrt{\frac{1}{2D_m} - 1}.$$

At this point, Eq. (33) has to be averaged over an oscillation period to obtain an expression for the averaged zonal drift velocity. The averaging requires the inclusion of the $O(a^2)$ shift, $ZA^2/2$, where $Z = -\frac{3}{4\omega_m^2}\left(\frac{1}{2D_m} - 1\right)^{1/2}$ in the solution for $\delta\varphi$ (see Ref. 16). This inclusion yields

$$\left\langle \frac{d\lambda}{dt} \right\rangle = (\gamma_3 + \gamma_1 Z)\frac{A^2}{2} = -\frac{A^2}{2}. \tag{34}$$

Thus, the averaged zonal drift velocity is governed by the $O(A^2)$ nonlinearity in the problem. Finally, a similar expansion around D_m and $\varphi_m = 0$ for $t > t_{cr}$ yields

$$\frac{d\lambda}{dt} = -\frac{1}{2} + D_m + \delta D + D_m\delta\varphi^2, \tag{35}$$

instead of Eq. (33). Thus, averaging over one period of oscillations yields

$$\left\langle \frac{d\lambda}{dt} \right\rangle = -\frac{1}{2} + D_m + D_m\frac{A^2}{2}. \tag{36}$$

Therefore, for $t > t_{cr}$, the averaged zonal drift velocity is mostly governed by the monotonic increase in the angular momentum $D_m(t)$ beyond its critical value 1/2 predicted by Eq. (18).

VI. ADDITIONAL FORMS OF WIND-STRESS FORCING

The analysis of the constant Γ case presented above is extended now to several cases of variable Γ using the same procedure.

A. $\Gamma(\varphi) \neq 0$ at all φ

Similar expressions can be derived for $\Gamma = G\cos\varphi$, in which case $dD_m/dt \approx G\cos^2\varphi_m = 2GD_m$ so the temporal evolution of D is given by

$$D_m = D_0 e^{2Gt}. \tag{37}$$

Here, only $G > 0$ is relevant since for $G < 0$, the value of D decreases with time so the column moves toward the pole, i.e., away from the equator. This equation yields the critical time for reaching the equator ($D = 1/2$) in this, $G > 0$, case,

$$t_{cr} = -\frac{\ln(\cos^2\varphi_0)}{2G}. \tag{38}$$

As an illustration, Fig. 3 shows the $\Gamma = G\cos\varphi$ case with the same G and initial conditions as in Fig. 2. Note the similar qualitative features of the dynamics in the two forms of Γ. The obvious difference is the value of t_{cr} that equals 59 when $\Gamma = G$ (Fig. 2) and 69 when $\Gamma = G\cos\varphi$ (Fig. 3). The higher value of t_{cr} in the latter case probably results from the lower mean strength of the wind forcing along the equatorward directed trajectory that implies lower speeds. Similar results, but with a different value of t_{cr}, were also obtained for $\Gamma = G\cos^2\varphi$ (results not shown).

B. $\Gamma(\varphi)$ changes sign

In this subsection, we analyze a particular case that quantifies the dynamical consequences of the existence of a latitude where the wind stress vanishes. The $\Gamma(\varphi)$ structure we examine is

$$\Gamma(\varphi) = G(\cos\varphi - \cos\hat{\varphi}), \tag{39}$$

for which Γ vanishes at latitude $\hat{\varphi}$.

The approximate analytic solution of $D_m(t)$ in this case is obtained by solving $dD_m/dt = G\cos\varphi_m(\cos\varphi_m - \cos\hat{\varphi})$. Substituting $\cos\varphi_m = \sqrt{2D_m}$ and integrating the resulting equation yields

$$|\cos\varphi_m - \cos\hat{\varphi}| = |\cos\varphi_0 - \cos\hat{\varphi}|e^{Gt}. \tag{40}$$

This equation shows that for $G < 0$, ϕ_m converges to $\hat{\varphi}$ at large times for any initial ϕ_0, while for $G > 0$, the trajectory always diverges away from $\hat{\varphi}$, i.e., for $\phi_0 > \hat{\phi}$, ϕ_m moves toward the pole, while for $\phi_0 < \hat{\phi}$, ϕ_m moves toward the equator, reaching it at the critical time, t_{cr}, of

$$t_{cr} = \frac{1}{G}\ln\frac{\cos\varphi_0 - \cos\hat{\varphi}}{1 - \cos\hat{\varphi}} \tag{41}$$

and staying there at all $t > t_{cr}$. This equatorial approaching case is similar to the scenario encountered in previous examples where Γ does not pass through 0. We illustrate all these possibilities in Figs. 4 and 5, which show the evolution of ϕ and λ in the numerical simulation for $G = -0.005$ and $G = 0.005$, respectively. The initial conditions in both figures are $u(0) = 0$, $v(0) = 0.02$, $\lambda(0) = 0$, and the blue and red curves in the figures show the cases $\varphi(0) = 1.2\hat{\varphi}$ and $\varphi(0) = 0.8\hat{\varphi}$, respectively.

The upper panel in Fig. 4 ($G < 0$) illustrates the convergence of φ to $\hat{\varphi}$ and the onset of instability as the amplitude of oscillations around the slowly varying φ_m increases. The lower panel in this figure illustrates the increase in the zonal drift with the increase in oscillations' amplitude [see Eq. (34)]. All these results are predicted by the analysis presented above. The evolution shown in Fig. 5 ($G > 0$) confirms the expected divergence of φ from $\hat{\varphi}$, when the wind forcing is directed eastward. The red lines in the two panels of this figure ($\phi_0 < \hat{\varphi}$) are similar to those in the example of Fig. 3, as described by the analysis. For instance, one observes the change in the character of evolution at $t_{cr} = 230$.

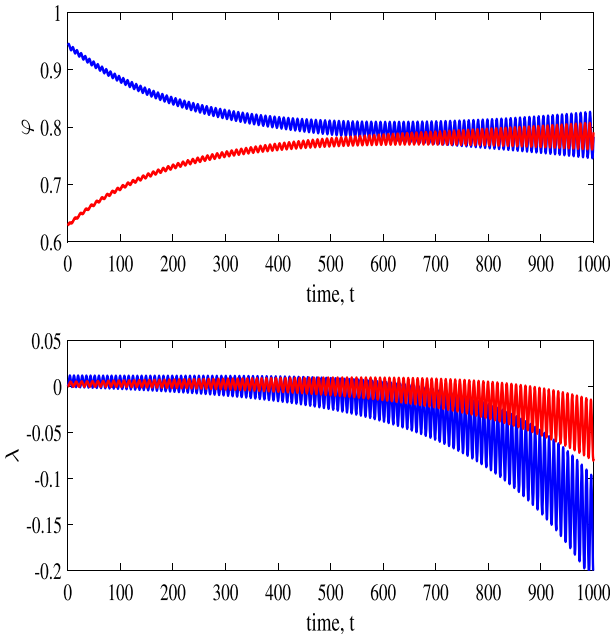

FIG. 4. The results of numerical simulation for Γ passing zero at $\hat{\varphi} = \pi/4$ with $G = -0.005$, $u(0) = 0$, $v(0) = 0.02$, $\lambda(0) = 0$. The blue and red lines show the cases $\varphi(0) = 1.2\hat{\varphi}$ and $\varphi(0) = 0.8\hat{\varphi}$, respectively. Upper panel: the temporal evolution of $\varphi(t)$. The blue and red trajectories merge at $\hat{\varphi}$ at later times, and the growing amplitude instability develops. Lower panel: the evolution of λ. The zonal drift increases with the increase in the amplitude of φ oscillations as predicted by the theory.

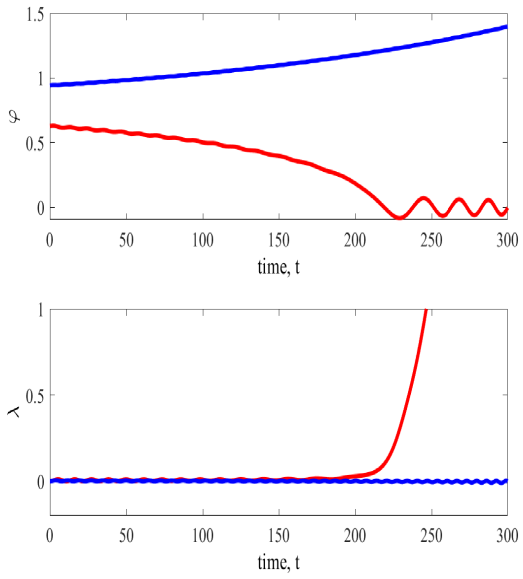

FIG. 5. The results of numerical simulation for Γ passing zero at $\hat{\varphi} = \pi/4$ for the same parameters and initial conditions as in Fig. 4, but with $G = 0.005$. The blue and red lines again show the cases $\varphi(0) = 1.2\hat{\varphi}$ and $\varphi(0) = 0.8\hat{\varphi}$, respectively. Upper panel: the evolution of $\varphi(t)$. Both blue and red trajectories diverge from $\hat{\varphi}$ at later times. Lower panel: the evolution of λ. The evolution of the red line is similar to that in Fig. 3 as φ reaches the equator and develops oscillations after the critical time, while λ increases rapidly after the critical time due to the monotonic increase in D_m for $t > t_{cr}$.

VII. SUMMARY AND DISCUSSION

The theory developed in this work is constructed based on the substitution of the angular momentum, D, for the zonal velocity, u, as a dependent variable of the system. This substitution yields a dynamical system view of the wind driven ocean flow, in which the trajectory of a water column is described by the motion of a quasiparticle in a time-dependent potential well. The potential's minima, φ_m, are determined by the corresponding value of the angular momentum, D_m, both of which vary slowly with time since the nondimensional amplitude of the wind forcing is $O(10^{-5})$. The rate of temporal variation of D and φ_m by the wind stress is several orders of magnitude slower than the (nondimensional) frequency of inertial oscillations around φ_m that equals $\sin\varphi_m$, which is $O(1)$ except for the immediate vicinity of the equator. The application of the adiabaticity theorem to the wind driven dynamical system ensures that φ remains near φ_m (including the global minimum, $\varphi_m = 0$, at large times) at all times provided $\varphi(t = 0)$ is near φ_m. The solution of the simple evolution equation $dD_m/dt = \Gamma\cos\varphi_m$ for the prescribed $\Gamma(\varphi_m)$ forcing then completes the elements required to close the theory.

The new theory yields explicit expressions for the time it takes a column that originates at an arbitrary latitude $\varphi(0)$ to reach the equator. In addition, it quantifies the rate of zonal drift, which has never been quantified before. Though the same equations were also simulated in Ref. 7, no analysis was attempted in that work (that included friction) and this is corrected in the present work. In particular, the present work relies on the small order of magnitude of the nondimensional wind stress that is over four order-of-magnitude smaller than the O(1) frequency of inertial oscillations.

The forcing in the present theory is a latitude dependent zonal stress, while its time and longitude dependence are neglected. The theory also ignores the dynamical consequences of meridional stresses. With the timescale of $1/2\Omega = 6/\pi$ hours, one week corresponds to less than 90 nondimensional time units in the present theory. In contrast, data recorded by buoys in various parts of the open ocean reveal mean (over several years) fairly large daily variations of wind speed and direction.[17,18] Thus, at the long times $[O(10^2$–$10^3)]$ examined here, the temporal and zonal variations of the zonal wind speed, as well as the meridional wind, should be incorporated in the theory prior to its application to any particular observation. Such a qualitative agreement with observations of three drifter trajectories in the Pacific Ocean is described in Ref. 7 where the Lagrangian model includes a zonal wind stress that varies with both longitude and latitude. Clearly, the present theory is only the first step in the challenging attempt to develop an analytic model of wind-driven transport in the ocean.

The theory and numerical results of Subsection VI B highlight the importance of the existence of latitude $\hat{\varphi}$ where the wind stress changes sign. A consideration based on the classical steady f-plane results[1] suggests that the wind-driven flow should diverge (converge) when Γ changes from positive to negative (from negative to positive) when it crosses $\hat{\varphi}$. However, as shown in Subsection VI B, the spherical counterpart of the theory yields an instability at that latitude so the amplitude of the (inertial) oscillations increases with time. This result

has observational consequences that can (and should) be verified in future dedicated field campaigns.

Though the wind stress forces the moving column at all $t > 0$, the (kinetic) energy of the column only oscillates when the Coriolis force does not vanish, i.e., as long as the column remains away from the equator. Once the column reaches the equator (which occurs at $t = t_{cr}$ for $G > 0$), the non-rotating dynamics applies, i.e., the column's zonal velocity, u, increases linearly with time so the longitude coordinate, λ, increases quadratically with time. These conclusions are evident in the numerical results shown by the red curve in the lower panel of Fig. 5.

The results derived in the present spherical theory for uniform Γ can be compared with those derived recently on the β-plane.[2] As evident from Eqs. (20) and (21), the fundamental difference between the two theories originates from the different temporal evolution of D, which is linear with Γ on the β-plane, while on the sphere, it is related to (and determines) φ_m. This mutual dependence of D_m and φ_m on the sphere results in the highly nontrivial dynamics (including linear instability) on the sphere. According to Eq. (34), on a sphere the zonal drift is directed westward as in inertial oscillations[5] since $O(G^2)$ terms (i.e., the direct effect of the wind stress) were neglected, which agrees with the results derived on the β-plane.

The time-dependent potential paradigm employed here by substituting the angular momentum for the zonal velocity can also be employed in a future theory that focuses on the effect of non-zonal, φ-dependent, wind stress. This setup is more challenging than the one employed here since a forcing term should be added to the RHS of the meridional momentum equation, Eq. (2) [and hence to Eq. (6) as well], which greatly complicates the expression of the potential in Eq. (12).

AUTHOR DECLARATIONS

Conflict of Interest

The authors have no conflicts to disclose.

Author Contributions

Nathan Paldor: Conceptualization (equal); Formal analysis (equal); Investigation (equal); Project administration (equal); Writing – original draft (equal); Writing – review & editing (equal). **Lazar Friedland:** Conceptualization (equal); Formal analysis (lead); Writing – original draft (equal); Writing – review & editing (equal).

DATA AVAILABILITY

Data sharing is not applicable to this article as no new data were created or analyzed in this study.

REFERENCES

[1]V. W. Ekman, "On the influence of the earth's rotation on ocean-currents," Ark. Mat., Astron. Fys. **2**, 1–52 (1905).
[2]N. Paldor and L. Friedland, "Extension of Ekman (1905) wind-driven transport theory to the β-plane," Ocean Sci. **19**, 93–100 (2023).
[3]P. Ripa, "'Inertial' oscillations and the β-plane approximation(s)," J. Phys. Oceanogr. **27**, 633–647 (1997).
[4]N. Paldor, "Inertial particle dynamics on the rotating Earth," in *Lagrangian Analysis and Prediction of Coastal and Ocean Dynamics*, edited by A. Griffa, A. Kirwan, Jr., A. Mariano, T. Özgökmen, and H. Rossby (Cambridge University Press, 2007), pp. 119–135.
[5]N. Paldor, "The zonal drift associated with time-dependent particle motion on the earth," Q. J. R. Meteorol. Soc. **127**, 2435–2450 (2001).
[6]N. Paldor and E. Boss, "Chaotic trajectories of tidally perturbed inertial oscillations," J. Atmos. Sci. **49**, 2306–2318 (1992).
[7]N. Paldor, "The transport in the Ekman surface layer on the spherical earth," J. Mar. Res. **60**, 47–72 (2002).
[8]A. Constantin and R. Johnson, "Ekman-type solutions for shallow-water flows on a rotating sphere: A new perspective on a classical problem," Phys. Fluids **31**, 021401 (2019).
[9]C. M. Bender, S. Orszag, and S. A. Orszag, *Advanced Mathematical Methods for Scientists and Engineers I: Asymptotic Methods and Perturbation Theory* (Springer Science & Business Media, 1999), Vol. 1.
[10]A. E. Gill, *Atmosphere-Ocean Dynamics* (Academic Press, 1982), Vol. 30.
[11]G. K. Vallis, *Atmospheric and Oceanic Fluid Dynamics* (Cambridge University Press, 2017).
[12]M. S. Longuet-Higgins, "The eigenfunctions of Laplace's tidal equation over a sphere," Philos. Trans. R. Soc., London, Ser. A **262**, 511–607 (1968).
[13]Y. De-Leon and N. Paldor, "Zonally propagating wave solutions of Laplace tidal equations in a baroclinic ocean of an aqua-planet," Tellus A **63**, 348–353 (2011).
[14]N. Paldor, Y. De-Leon, and O. Shamir, "Planetary (Rossby) waves and inertia–-gravity (Poincaré) waves in a barotropic ocean over a sphere," J. Fluid Mech. **726**, 123–136 (2013).
[15]V. Rom-Kedar, Y. Dvorkin, and N. Paldor, "Chaotic Hamiltonian dynamics of particle's horizontal motion in the atmosphere," Physica D **106**, 389–431 (1997).
[16]L. D. Landau and E. M. Lifshitz, *Mechanics*, 4th ed. (Elsevier, 1982).
[17]Z. Shu, Q. Li, P. Chan, and Y. He, "Seasonal and diurnal variation of marine wind characteristics based on lidar measurements," Meteorol. Appl. **27**, e1918 (2020).
[18]F. J. Turk, S. Hristova-Veleva, and D. Giglio, "Examination of the daily cycle wind vector modes of variability from the constellation of microwave scatterometers and radiometers," Remote Sens. **13**, 141 (2021).